

# DIRECT SIMULATION OF TURBULENCE GENERATION AND TRANSFORMATION IN FLOWS OBSTRUCTED BY SQUARE GRIDS

Nagihan Özyilmaz, Kamen N. Beronov  
Lehrstuhl für Strömungsmechanik, Universität Erlangen-Nürnberg  
Cauerstr. 4, D-91058 Erlangen, Germany  
{noezyilm,kberonov}@lstm.uni-erlangen.de

## ABSTRACT

Flows through stationary, square grids are examined numerically at moderate Reynolds numbers using direct numerical simulation with a standard lattice BGK method. Beside turbulent energy decay, the anisotropy and cross-flow inhomogeneity of Reynolds stress components is studied. It is found that near the grid region the levels of the latter quantities are high, in the adjacent intermediate region they decay, and in a region of final decay of turbulence, inhomogeneity increases again while anisotropy continues to decay, well described by power laws with exponents  $-1/6$  and  $+1/4$  respectively. In all regions, both quantities have comparable magnitudes; for dimensionless downstream distribution  $x/M > 5$ , they are small ( $< 5\%$ ).

## INTRODUCTION

Grid-generated turbulence (GGT) is an extensively studied area of basic turbulence research. While a large number of experimental studies exists on the subject, very few numerical studies are known so far. For the experimental studies, see e.g. Grant and Nisbet (1957), Comte-Bellot and Corrsin (1966,1971), Gence and Mathieu (1979,1980), Han (1988), Jovanovic *et al.* (2003). A direct investigations of GGT (as opposed to homogeneous decaying turbulence) like the one by Djenidi (2006) are rare. In all those studies, the main focus is on the presumably existent universal spatial decay law for turbulent kinetic energy. In some studies, return to isotropy rates and the influence of contractions on anisotropy are issues of interest. Here, we focus on another characteristic of GGT, comparing two important nondimensional descriptors of GGT - the anisotropy of Reynolds stresses (ARS) and the inhomogeneities of Reynolds stresses, normal to the mean flow (NIRS). Although each of these plays an important role in GGT, there is no published study, where their magnitudes are discussed in the same context. The streamwise inhomogeneity, complementary to NIRS, is closely related to spatial decay of kinetic energy, for which our detailed data suggest — despite the relatively low Reynolds numbers simulated — a clear-cut power law exponent. But the main finding to be presented here is that both ARS and NIRS have quite comparable levels in GGT.

## NUMERICAL SET-UP

Two independent series of direct numerical simulations were carried out, using a lattice Boltzmann method with standard BGK relaxation and the  $D3Q19$  lattice model — see Frisch *et al.* (1986), Qian *et al.* (1992), He and Luo (1997), Gladrow (2000), Bouzidi and d’Humières (2001), Lallemand and Luo (2000), Zou *et al.* (2005). An MPI version of a code based on this method was applied, which has been described in Lammers *et al.* (2004).

In both simulations, referred to as Run 1 and Run 2, the same computational domain and geometry of the turbulence-generating grid were used: The uniform computational mesh had 2400 points in the streamwise and 160 points in the normal and in the spanwise direction. The grid consisted of identical rods with square cross section, a stride of  $M = 40$  in mesh step units, and rod side length  $d$  chosen such that  $d/M = 0.15$ , which resulted in a blockage ratio of  $\sigma = 0.28$ . Periodic boundary conditions were applied in each of the three main spatial coordinate directions. The grid was placed orthogonally to the main flow direction, as defined by a constant spatial driving force vector. The only difference between the two simulations was the magnitude of that driving “pressure drop,” resulting in Reynolds numbers  $Re_m = 1400$  and  $Re_m = 2000$  based on the time and space-averaged mean velocity and the mesh stride  $M$ .

In preliminary simulations, the length of the flow domain was iteratively adjusted to assure that a sufficient decay of turbulent energy (over four orders of magnitude) took place along the flow domain, so that the reentering flow resulting from the periodic boundary condition in the mean flow direction had the physical significance of an infinitesimal perturbation only. In addition, a region of artificial, linear damping of deviations from the mean flow velocity direction and magnitude was introduced in the spatial region ahead of the grid, where the turbulence magnitudes had their minimum anyway. It was verified that this measure not only reduced turbulence levels but also destroyed the natural flow structure and correlations of “outflowing” GGT and that it did not influence the quality of flow simulation in the region of interest, especially at and in the near downstream vicinity of the grid.

## RESULTS

It is well known, already since Batchelor’s theoretical treatment and the early experimental measurements in GGT, that all its one-point statistics are componentally axiymmetric with respect to the mean flow direction. Our simulation data confirmed this, as well, to a precision well below the statistical noise level, for all statistics calculated. In particular, all off-diagonal components of Reynolds stress tensor are vanishingly small and the two components normal to the mean flow direction  $x$  are essentially equal. (A discussion of higher-order statistics is not of interest here.) Figure 1 compares the time-averaged Reynolds stress components  $\overline{v'^2}$  and  $\overline{w'^2}$ , in the  $y$  and  $z$  direction, respectively) obtained from both simulations. We may thus restrict the discussion to the anisotropy and the inhomogeneity of  $\overline{u'^2}$  and  $\overline{v'^2}$ .

## Turbulent energy decay

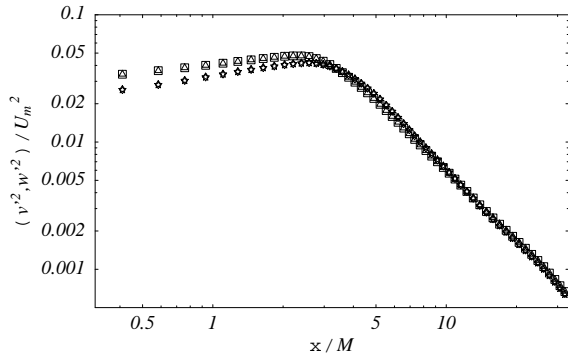


Figure 1: Comparison of longitudinal evolutions of time-averaged Reynolds stress components  $\overline{v'^2}$  and  $\overline{w'^2}$  for Run1 and Run2; diamonds:  $\overline{v'^2}$  and stars:  $\overline{w'^2}$  in Run 1, squares:  $\overline{v'^2}$  and triangles:  $\overline{w'^2}$  in Run 2.

An untrivial indication by Figure 1 is that GGT may obey a universal power law decay of turbulent kinetic energy for  $x/M > 5$ . This is strongly supported by further observations from our data, the beginning of the universal decay region being somewhat dependent on the statistic investigated, but always in the range  $5 < x/M < 10$ .

These and other data (at other Reynolds numbers or grid strides, to be summarized elsewhere) suggest a universal exponent of  $-5/3$  for this power law to within statistical error. That is, the turbulent kinetic energy  $k$  appears to decay as  $k \approx A(x/M)^{-5/3}$  with a prefactor depending on  $Re_m$ , grid stride  $M$ , rod geometry, inflow turbulence level and structure, etc. It can be argued theoretically (the details are presented in a separate publication) that this exponent is uniquely determined by a small set of physical assumptions, similar in nature to, but still clearly distinct from those proposed by Kolmogorov in his famous derivation of the energy cascade law for statistically steady homogeneous isotropic turbulence. In the present case, there is no homogeneity and the law applies only for low-level, “final decay” turbulence sufficiently far away from the generating grid. This is an analogy to the requirement of scale separation from the energy-containing range in isotropic turbulence. The power law presenting here, however, concerns not the intrinsic length scale of turbulence (eddy wave number), but an external, global scale (distance from the grid). The analog of “Kolmogorov scale” would be a (very large) distance after the grid, beyond which an exponential decay, as suggested by the well known theory of the “final period of decay” in homogeneous turbulence, sets in. We have not had the resources and intention to search for such a regime.

### Spatial evolution of anisotropy

The anisotropies of Reynolds stress components studied, are defined as usual by

$$a_{11} = \frac{\overline{u'^2}}{2k} - \frac{1}{3}, \quad a_{22} = \frac{\overline{v'^2}}{2k} - \frac{1}{3}, \quad (1)$$

where  $k$  is calculated from same the time-averaged Reynolds stresses and  $a_{22} = -a_{11}/2 < 0$ . Figure 2 shows the absolute values of  $a_{22}$ . Anisotropies decrease continuously after turbulence leaves the grid, even in the “final decay” region discernible in our data at  $x/M > 20$ , where perhaps the recirculating boundary condition rather than an approach to an exponential decay region corresponding to the “final period of decay” in homogeneous turbulence is having a dominant influence.

Comparison between the two runs shows only a small influence by the Reynolds number, more pronounced for the “vertical” component  $\overline{v'}$ . Although there is a difference in magnitude between different components of the anisotropy tensor, their decay obeys the same law and for  $x/M > 15$  this can be approximated by a clear power law whose exponent is approximately  $1/6$ .

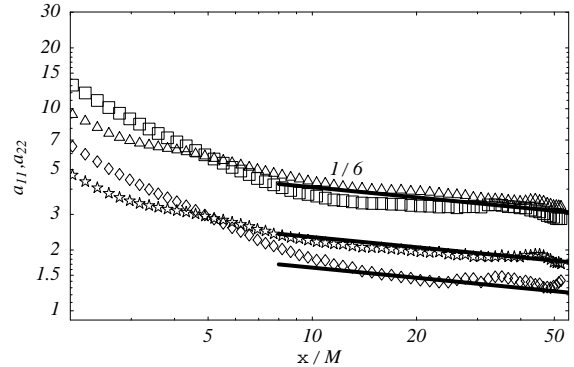


Figure 2: Longitudinal evolution of anisotropy tensor: squares:  $a_{11}$  and diamonds:  $|a_{22}|$  in Run 1, triangles:  $a_{11}$  and stars:  $|a_{22}|$  in Run 2.

An equally acceptable fit is given by an alternative logarithmic decay law (not shown). The situation is reminiscent of the still ongoing dispute whether developed turbulence along a flat wall obeys the classical log-law or a Reynolds-number-dependent power-law. Our opinion on the latter issue has been stated elsewhere and it would be imprudent to carry the debate over to the present case of GGT before the other observations that can be made from our data and are brought forward here have been independently verified and accepted.

### Inhomogeneity

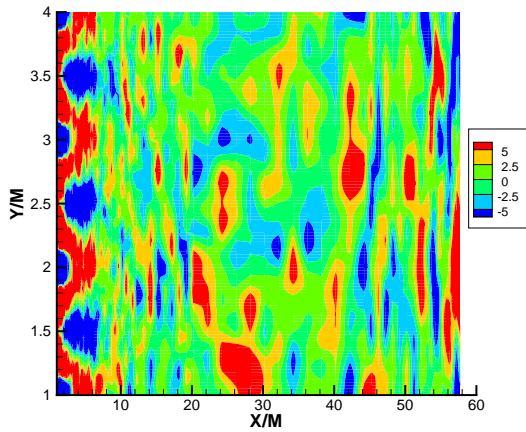
Following a suggestion for a measure of cross-sectional inhomogeneities forwarded by Ertunc and Lienhart (2006) and Ertunc (2007), we calculate the spatial distributions of the following indicator fields:

$$\overline{u'^2}(x, y) = \frac{1}{N} \sum_{j=1}^N \int_0^T \frac{dt}{T} \langle \overline{u'^2}(x, y, z_j, t) \rangle, \\ NIu(x, y) = \left( \frac{\overline{u'^2}(x, y)}{\frac{1}{N} \sum_{i=1}^N \overline{u'^2}(x, y_i)} - 1 \right) 100\%, \quad (2)$$

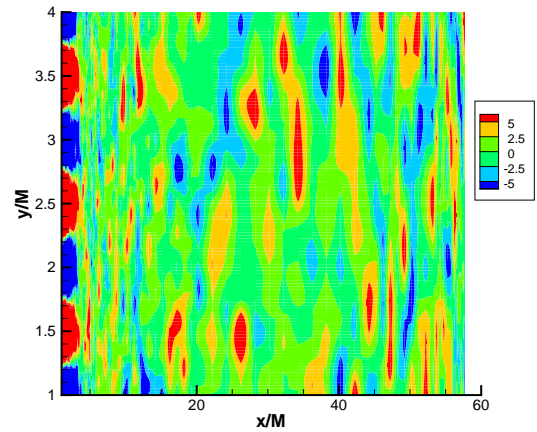
where  $i$  and  $j$  are any point in streamwise and normal directions respectively and  $N = 160$ . Similar equations can be derived for  $\overline{v'^2}(x, y)$  and  $NIv(x, y)$ .

Figure 3 and 4 show that, as expected, the highest niveau of inhomogeneity is observed immediately after the grid. It reaches approximately the level of 5% in both runs (and of course, for both inhomogeneity components).

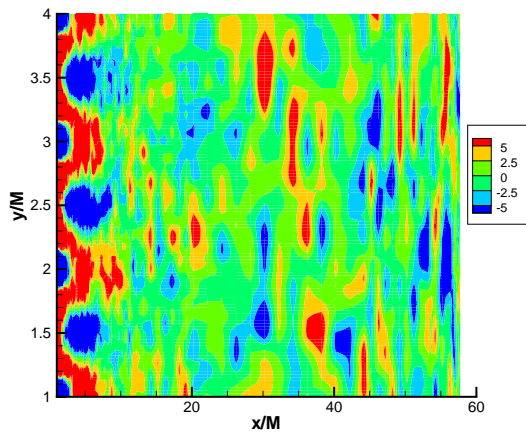
Anticipating a universal behaviour in the “final decay region” as identified in the previous section, it is of specific interest to follow the spatial evolution of the inhomogeneity indicators in that region of GGT. To that end, the values shown in Figure 3 and Figure 4 are averaged in the “vertical direction”  $y$ , at a fixed  $x/M$  position, to obtain the values which depend on the streamwise location only,  $i_{11}(x) = \frac{1}{N} \sum_{j=1}^N NIu(x, j)$  and  $i_{22}(x) = \frac{1}{N} \sum_{j=1}^N NIv(x, j)$ . The result is shown in Figure 5, for both components and both



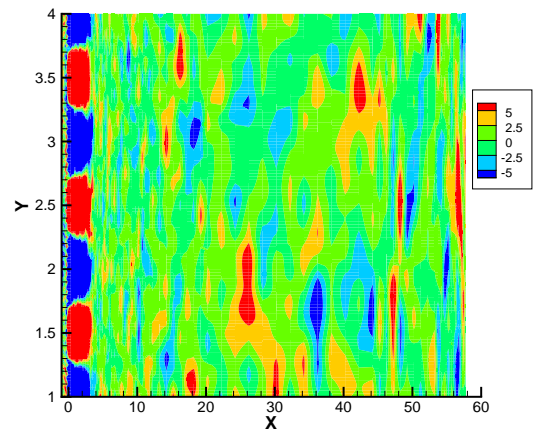
(a)



(a)



(b)



(b)

Figure 3: Distribution of  $NIu(x, y)$  %: a) Run 1, b) Run 2.

runs. After the grid, both components start to decay immediately. This decrease goes on until  $x/M \approx 15$  for the streamwise component, in both runs. But for  $x/M > 15$ , an — at first sight surprising — increase rather than a saturation of inhomogeneity is observed. For the “vertical” component of Reynolds stress tensor, this increase of the inhomogeneity starts at an earlier point,  $x/M > 8$ .

This observed increase of inhomogeneity in the “final decay region” of the GGT is not truly surprising, however, in view of the expected growth, in mean flow streamwise direction, of all spatial scales of the large mean flow structures found in the “later stages” of GGT. Such growth can indeed be seen in Figure 6(b). There, the time-averaged streamwise mean velocity is plotted on the mean-flow cross-sectional  $y - z$  plane at  $x/M = 30$ . The difference between the structure of this later stage and the near grid structure is clear, cf. Figure 6(a).

In an attempt to quantify this increase in cross-stream inhomogeneity, a power law has been found to give a rather acceptable prediction, when its exponent is approximately  $1/4$  — for both components and for both investigated Reynolds numbers. The coefficient of the power law is of course different for the different components, but for a specific component, it is found to be approximately the same for different

Figure 4: Distribution of  $NIv(x, y)$  %: a) Run 1, b) Run 2.

Reynolds numbers.

### Comparison between anisotropy and inhomogeneity

The magnitudes of the anisotropies and the inhomogeneities of both components of the Reynolds stress tensor are comparable at any given position  $x/M$ , as illustrated by Figure 7. Here, only the quantities for Run 1 are shown, but the trend is the same for Run 2.

Figure 7(a) compares the two quantities for the streamwise component and Figure 7(b) compares them for the vertical component. The highest anisotropy and inhomogeneity levels are found in the region directly after the grid, as expected. Both components follow an almost constant line until  $x/M \approx 2$ . For the streamwise component, the highest level for anisotropy is around 10% in this region and for inhomogeneity about 20%. This value for streamwise component is very close to the one observed for normal component. The difference in the componental behaviour with respect to anisotropies is larger, it is 6% for the vertical component. As seen clearly by this study, the inhomogeneity starts from a higher niveau than the anisotropy level for both components. However,  $i_{11}(x)$  starts to fluctuate more or less in the same region with  $a_{11}$  for  $x/M > 5$ . In the “final decay region,” there is still a clear level difference between  $i_{22}(x)$  and  $a_{22}$ .

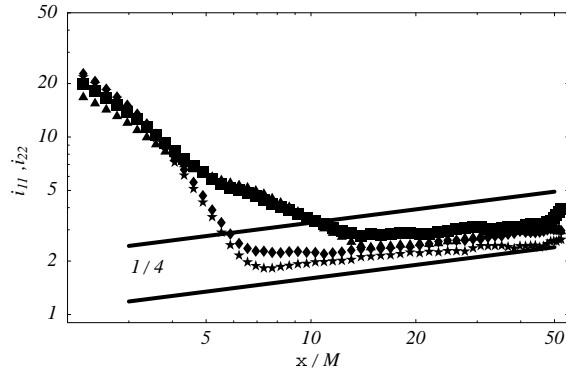


Figure 5: Longitudinal evolution of  $i_{11}(x)$  and  $i_{22}(x)$ ; squares:  $i_{11}(x)$  and diamonds:  $i_{22}(x)$  for Run 1, triangles:  $i_{11}(x)$  and stars:  $i_{22}(x)$  for Run 2.

But, they are in comparable orders: 1.5% for  $a_{22}$  and 3% for  $i_{22}(x)$ .

### CONCLUSIONS AND OUTLOOK

Grid-generated turbulence (GGT) was examined with respect to componental anisotropy of Reynolds stresses (ARS) and to cross-flow spatial inhomogeneity (NIRS) at two moderate Reynolds numbers. It was found that, at a given downstream position, the magnitudes of both dimensionless characteristics are of the same order at both Reynolds numbers. It was suggested that the decay of ARS in the “final decay region” of GGT could be well described by a power law with an exponent of  $1/6$ . The same type of law could also be applied for the increase of NIRS in the same region with an exponent of  $1/4$  for both components and at both Reynolds numbers.

In future work, the observed increase in the “final period” could be addressed in detail, by extending the computational domain in both directions normal to the mean flow direction, in the expectation of the existence of a region of exponential decay of turbulent energy at nearly preserved anisotropy. Such a study would require a domain of the size  $2400 \times 400 \times 400$ .

### REFERENCES

Benzi R., Succi S., and Vergassola M., 1992, “The lattice Boltzmann equation: Theory and applications”, *Phys. Rev. Lett.*, Vol. 222, pp. 145-197.

Bhatnagar P.L., Gross E. P., Krook M., 1954, “A model for collision processes in gases. I. Small amplitude processes in charged and neutral one-component systems”, *Phys. Rev.*, Vol. 94, pp. 511-525.

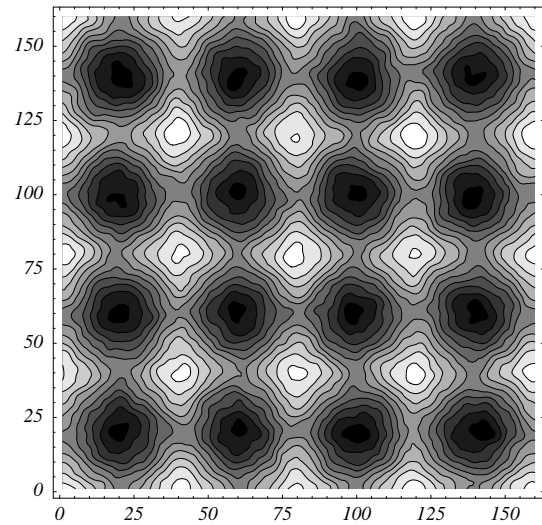
Bouzidi M., and d’Humières D., 2001, “Lattice Boltzmann equation on a two-dimensional rectangular grid”, *J. Comput. Phys.*, Vol. 172, pp. 704-717.

Comte-Bellot G., and Corrsin S., 1966, “The use of a contraction to improve the isotropy of grid generated turbulence”, *Journal of Fluid Mechanics*, Vol. 25, pp. 657.

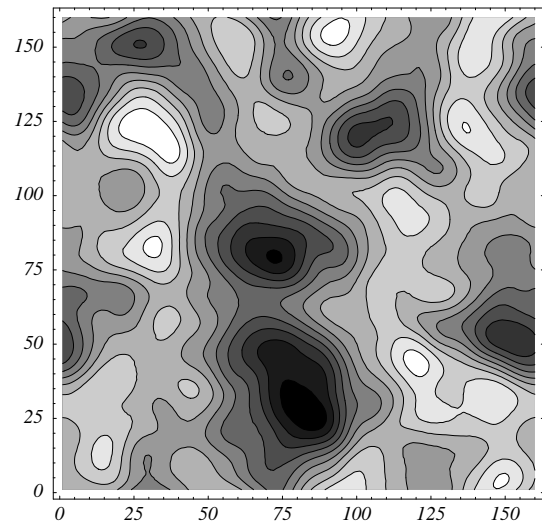
Comte-Bellot G., and Corrsin S., 1971, “Simple Eulerian time-correlation of full- and narrow-band velocity signals in grid-generated, isotropic turbulence”, *Journal of Fluid Mechanics*, Vol. 48, pp. 273-337.

Djenidi L., 2006, “Lattice-Boltzmann simulation of grid-generated turbulence”, *Journal of Fluid Mechanics*, Vol. 552, pp. 13-35.

Ertunc Ö., and Lienhart H., 2006, Inhomogeneity of grid-



(a)



(b)

Figure 6: Local mean flow structures on  $y - z$  plane for Run 1: a)  $x/M = 2.5$ , b)  $x/M = 30$ .

generated turbulence under zero-strain and finite strain”, *LSTM Erlangen, Report*.

Ertunc Ö., 2007, “Experimental and numerical investigations of axisymmetric turbulence”, *PhD thesis, LSTM erlangen*.

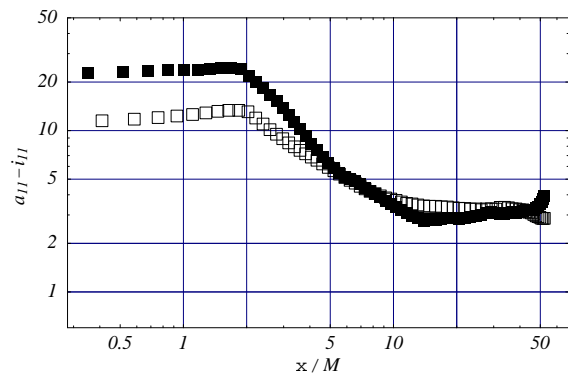
Frisch U., d’Humières D., and Pomeau Y., 1986, “Lattice-Gas automata for the Navier-Stokes equation”, *Phys. Rev. Lett.*, Vol. 56, pp. 1505-1508.

Gence J. N., and Mathieu J., 1979, “On the application of successive plain strains to grid-generated turbulence”, *Journal of Fluid Mechanics*, Vol. 93, pp. 501-513.

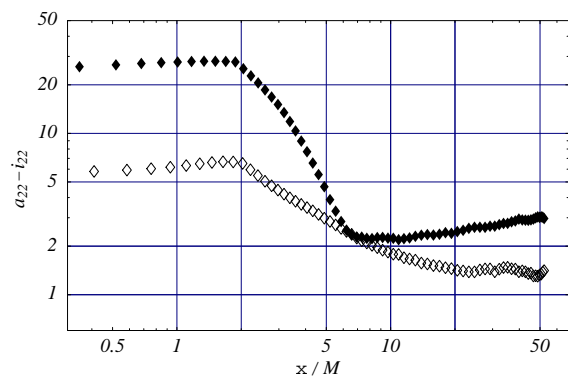
Gence J. N., and Mathieu J., 1980, “The Return to Isotropy of a homogeneous turbulence having being submitted to two successive plane strains”, *Journal of Fluid Mechanics*, Vol. 101, pp. 556-566.

Gladrow D. A. W., 2000, “Lattice-Gas cellular automata and lattice Boltzmann Models”, *Springer-Verlag, Berlin*.

Grant H. L., and Nisbet I. C. T., 1957, “The inhomogeneity of grid turbulence”, *Journal of Fluid Mechanics*, Vol. 2,



(a)



(b)

Figure 7: Comparison between Reynolds stress anisotropies and inhomogeneities for Run 1. a) open squares:  $a_{11}$ , closed squares:  $Inh(u'^2(x))$ , b) open diamonds:  $a_{22}$ , closed diamonds:  $Inh(v'^2(x))$ .

pp. 263-272.

Han Y. O., 1988, "The Effect of contraction on grid generated turbulence", *PhD thesis, State university of New York at Buffalo*.

He X., and Luo L. S., 1997, "Theory of the lattice Boltzmann method: From the Boltzmann equation to the lattice Boltzmann equation", *Phys. Rev. E*, Vol. 56, pp. 6811.

Jovanovic J., Otic L., and Bradshaw P., 2003, "On the anisotropy of axisymmetric strained turbulence in the dissipation range", *Journal of Fluids Engineering*, pp. 401-413.

Lallemand P., and Luo L. S., 2000, "Theory of the lattice Boltzmann method: Dispersion, dissipation, isotropy, Galilean invariance, and stability", *Phys. Rev. E*, Vol. 61-6, pp. 6546-6562.

Lammers P., 2004, "Direkte numerische Simulationen wandgebundener Stroemungen kleiner Reynoldszahlen mit dem lattice Boltzmann Verfahren", *PhD thesis, LSTM erlangen*.

Qian Y. H., d'Humirés D., and Lallemand P., 1992, "Lattice BGK models for Navier-Stokes equation", *Europhys. Lett.*, Vol. 17, pp. 479.

Zou Q., Hou S., and Doolen G. D., 1995, "Analytical solutions of the lattice Boltzmann BGK model", *J. Stat. Phys.*, Vol. 81, pp. 319-334.